J Fluoresc (2012) 22:1291–1300
DOI 10.1007/s10895-012-1071-z

ORIGINAL PAPER

Two-Photon Activated Two-Photon Fluorescence and Binding of Azidocoumarin in a Gelatin Matrix

Stefan V. Stoianov · Hans D. Robinson

Received: 4 December 2011 / Accepted: 29 May 2012 / Published online: 19 June 2012
© Springer Science+Business Media, LLC 2012

Abstract We study the creation of fluorescence patterns inside a gelatin gel by way of two-photon photoactivation of 7-azido-4-trifluoromethyl-1,2-benzopyrone (azidocomarin 151) contained in the gel matrix. As ultrafast light pulses are focused into the gel, onset of two-photon fluorescence, highly nonlinear in the applied optical power, is observed as azidocoumarin is converted into a fluorescent dye that binds to the gelatin. We fit the time dependence of the fluorescence to a model that incorporates the competition between coumarin photoactivation and photobleaching as well as the gradual degradation of the gel when it is exposed to the high intensity laser light. The model predicts that the initial rate of fluorescence onset should scale as the P^4, where P is laser power, while the signal at long exposure time should scale as $P^{3/2}$. The observed exponents are 4.18 and 1.34, respectively. The model allows us to estimate the cross section and quantum yield of two-photon induced photobleaching of azidocoumarin 151. The numerous technical uses of gelatin and the collagen from which it derives in areas ranging from photography to tissue engineering provide possible applications for the techniques described in this paper.

Keywords Photoactivation · Photobleaching · Fluorescence patterning · Azidocoumarin · Gelatin

Introduction

Photoactivatable fluorophores, i.e. compounds and other entities that may transform into a fluorescent form on absorption of a photon, have gained in interest in the last few years due to their use in optical superresolution microscopies such as PALM [1], FPALM [2] and STORM [3]. The toolbox of controllable emitters includes fluorescent proteins [4, 5], various types of small organic molecules [6, 7] and even quantum dots [8]. Aryl azides is a class of compounds where some members have this property, the first and most well-known example is 7-azido-4-methyl-1,2-benzopyrone (azidocoumarin 120, AzC120), although a number of other such molecules have recently been synthesized [9]. These compounds, like other aryl azides, become highly reactive upon photoactivation (also known as photo-uncaging), and readily form bonds with a number of different moieties, including amines, active hydrogens, and unsaturated C=C bonds. Aryl azides that are subject to photoactivated fluorescence can therefore be used as fluorescent reporter molecules, as is the purpose of the commercially available crosslinker SAED [10].

Photoactivation usually occurs on absorption of one UV photon, but if the light intensity is high enough, it can also be triggered by simultaneous absorption of two photons, each carrying half the energy required to excite the molecule. This is a nonlinear process where the efficiency scales with light intensity, which means that it can be limited almost completely to the volume immediately surrounding the focus of a converging light beam. Two-photon uncaging enables superresolution microscopy in three dimensions [11] on thick samples, while other approaches [12–14] are limited to relatively thin slices. The two-photon process is also less photo-toxic to biological samples, creates less photobleaching, and enables imaging deeper inside tissue than is possible with shorter excitation wavelengths. For these reasons, the nonlinear optical properties of a number of different photoactivatable fluorescent compounds have been investigated [7], although it appears that no aryl azides have been studied to date.

S. V. Stoianov · H. D. Robinson (✉)
Department of Physics, Virginia Tech,
910 Drillfield Drive,
Blacksburg, VA 24061, USA
e-mail: hansr@vt.edu

The localization of nonlinear optical processes to a focus also underlies microstructure fabrication using two-photon induced polymerization [15, 16]. In that technique, the focus is scanned throughout a photosensitive gel, causing it to crosslink in a 3D pattern determined by the movement of the beam focus, allowing arbitrary shapes to be fabricated with sub-micrometer resolution.

In this paper, we apply the same technique to create arbitrary patterns of fluorescence in a gelatin gel where azidocoumarin has been incorporated. Photoactivation causes the dye to bind to the protein matrix while simultaneously becoming fluorescent, creating a static pattern of fluorescence at the focus. Most of the other reaction products are rapidly removed from the illuminated spot by diffusion, and therefore play no further role in the experiment. Visualization of the fluorescence is also accomplished through two-photon absorption, which makes it possible to carry out both photoactivation and fluorescence monitoring locally at any point in the gel. It is then possible to immediately visualize the written pattern, without waiting for a development step. We note that coumarins can be used as photo initiators of polymerization [17–20], so this approach may also be of direct interest to the field of two-photon fabrication.

In addition to photoactivation and fluorescence, the optical signal we observe is also affected by photobleaching of the dye bound to the matrix. All three process are initiated by two-photon absorption, which leads to a strongly nonlinear behavior in the onset and saturation of the fluorescence we observe. Here, we present a model for the time evolution of the onset of fluorescence that occurs when a fs laser is focused inside the gel. At short time scales, the model fits our data very well, and allows us to estimate the two-photon cross section for photobleaching of the dye. At longer times, the model fails, partly due to the use of a Gaussian beam approximation, but mainly because the gel's ability to bind the activated dye degrades as it is exposed to high intensity laser light for a prolonged period of time. A simple threshold-type model describing how the damage to the gel affects the fluorescence signal remedies this failure within the experimental resolution of our data.

Gelatin is a hydrolyzed form of collagen, which is by far the most abundant protein in the human body [21], making up 30 % or more of its protein content. Collagen and gelatin have numerous technical uses which may provide applications for the technique discussed in this paper. For example, collagen is one of the materials used to make tissue engineering scaffolds [22], and patterned two-photon activation of dyes such as azidocoumarin could be used to create fluorescent signposts inside such a scaffold, which could be used to identify specific points that can then be repeatedly monitored during tissue growth.

The photoactivatable compound used in this work was 7-azido-4-trifluoromethyl-1,2-benzopyrone (azidocoumarin 151, AzC151) which was chosen over the better studied AzC120 moiety because the additional fluorine atoms in AzC151 redshifts the absorption band, improving the overlap with the wavelength range of our laser.

Experimental

In the basic experiment showcased in this paper, we incorporate AzC151 into a gel made from water, methanol and gelatin, and monitor its behavior as it is activated by a beam of focused light from a femtosecond light source. Figure 1 schematically shows the optical setup. Pulses from a Chameleon Ultra II ultrafast Ti:Sapph laser are focused with an inverted Zeiss LSM 510 laser scanning confocal microscope into the sample gel. The gel is contained in an airtight container to prevent evaporation of the solvent, and optical

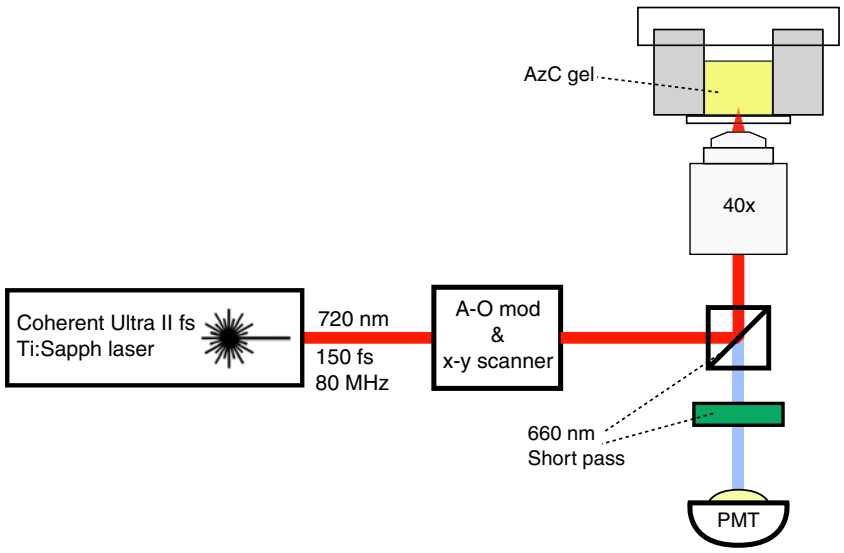

Fig. 1 Schematic of the experimental setup. 150 fs wide pulses from a Chameleon Ultra II Ti:Sapph ultrafast laser go through an acousto-optical modulator and an x-y scanner (which permits fast scanning of the beam inside the sample). A Zeiss LSM 510 confocal microscope is used to focus the laser pulses inside an azidocoumarin-laced gelatin gel contained in an airtight capsule. Two-photon fluorescence is collected in reflection mode and filtered out from the laser light with a beamsplitter and shortpass optical filter before being detected by a photo multiplier tube (color online)

access is provided through a thin glass window at the bottom of the container. Any resulting fluorescence is collected by the microscope objective, and separated from the laser light with a beam splitter and an optical long pass filter, before being detected by a photomultiplier tube. The laser outputs 150 fs long pulses at 80 MHz and can be tuned to any wavelength between 680 nm and 1,080 nm. The power of the laser was measured before entering the microscope and at the backplane of the microscope objective. These numbers, along with the transmittance of the objective provided by the manufacturer, were used to calculate the total optical power delivered to the gel.

Scheme 1 outlines the reaction paths for **1** (Azidocoumarin 151, AzC151). Upon absorption of a UV photon, **1** may expel a nitrogen molecule, forming a highly reactive nitrene **2**. The nitrene can then undergo ring expansion, incorporating the nitrogen atom into a dehydroazepine **3**, which then can react with nucleophiles to form the crosslinked product **4**. The nitrene can also react directly with a number of different groups and form crosslinked products like **5**. Finally, the nitrene may directly abstract hydrogen or oxygen from the environment, reverting back to the original coumarin dye **6** or its nitrosubitituted version **7** [9]. The path to **3** and **4** normally dominates, but it can be suppressed if electron withdrawing moieties are attached to the aryl group [23], stabilizing the intermediate nitrene, so that products **5** and **6** also likely form in significant quantities [24]. This is an additional reason for chosing to work with AzC151 rather than AzC120 which lack the trifluoromethyl group in **1**. Among the photoreaction products, **5** and **6** are strongly fluorescent, while **3**, **4** and **7** are not. Therefore, it is likely that most of the fluorescence observed by us likely originates from **5**, although it is possible that **6** also contributes to the extents that it is fixed to the gel via hydrogen bonding.

The azidocoumarin was synthesized from its corresponding coumarin fluorescent dye by following the method of Barral et al. [25] Briefly, 100 mg of 7-amino-4-trifluoromethyl-1,2-benzopyrone (coumarin 151, C151) was dissolved in 10 ml of acetonitrile in a small round bottom flask. The solution was cooled to 0 °C and 110 µl *t*-butyl nitrite followed by 95 µl azidotrimethoxysilane were added dropwise. The reaction was allowed to proceed for 2 h in the dark after which it was dried, resulting in approximately 80 mg of a pinkish powder that was used without further purification. All chemicals were obtained from Sigma-Aldrich.

Gelatin gels are normally made from aqueous solutions, but since azidocoumarin is poorly soluble in water a 70:30 v/v mixture of water and methanol was used instead. It is known that a gelatin sol/gel system that contains alcohol exhibits phase separation by spinodal decomposition, but by using sufficiently high fractions of gelatin and water in the gel, this is suppressed as the critical decomposition temperature is pushed below the gel point [26]. In our case, we dissolved 13 mg of azidocoumarin in 45 ml of the solvent mixture, and added 7 g of type B gelatin (Sigma-Aldrich). The mixture was heated to about 45 °C and stirred for 20 min, and was then allowed to set. The gel was then reheated and sealed inside the airtight container before measurements were performed. If this container is kept in the dark and at room temperature, the optical properties of the gel remain stable for several weeks.

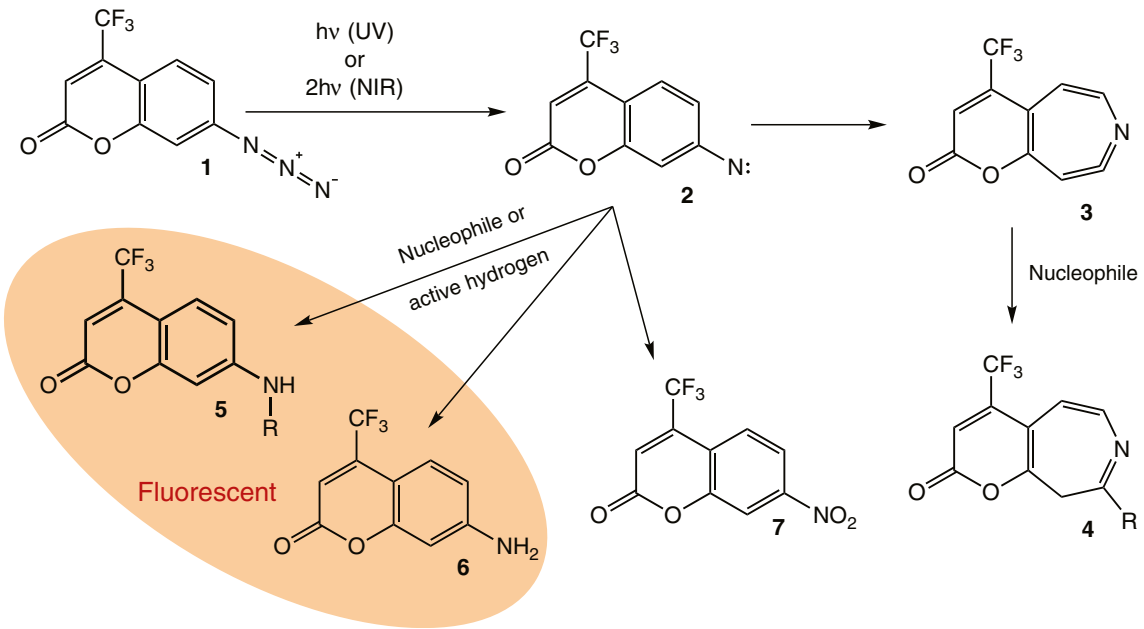

Scheme 1 Some possible reaction pathways for photoactivation of azidocoumarin 151 **1**. The fluorescent product **5** is crosslinked with the gelatin matrix and is responsible for the fluorescent signal we observe (color online)

Results and Discussion

Optical Characterization

Figure 2 shows the optical absorptivity spectra of azidocoumarin 151 as it is activated by UV light at 365 nm (black lines). The normalized fluorescence spectrum of the fully activated azidodoumarin is also shown (dotted line) along with the absorptivity and fluorescence spectra of coumarin 151 (solid and dashed grey lines). The absorptivity measurements were performed on a 70:30 water:methanol solution containing 50 μM AzC 151 or C151. 20 g/l of Gelatin B was also added to the AzC solution to provide a binding substrate for the activated dye. To avoid phase separation in the gelatin, the measurements were carried out at a temperature of about 35 °C. The AzC fluorescence spectrum was collected from the same 1 mM AzC gelatin gel as was used in the patterning experiments described below. The C151 fluorescence spectrum was obtained from a 70:30 water:methanol solution containing 1 mM of the dye.

The UV light causes the peak at 330 nm in Fig. 2 to disappear while a peak at 370 nm emerges. This peak shows good overlap with the absorption peak of C151 in a similar environment. The overlap is not perfect, nor is the absorptivity as high, which is expected given that the AzC converts into multiple products upon exposure to light. The fluorescence spectrum from activated AzC is on the other hand almost identical to the C151 fluorescence spectrum, consistent with Scheme 1.

Fluorescence Onset and Patterning

When the ultrafast laser is focused at a point in the gel, azidocoumarin in the focal spot is photoactivated. We are using light with a wavelength of 720 nm, so this occurs exclusively through two-photon absorption. The gelatin provides numerous binding sites for the activated coumarin, which with high probability binds to the gel close to the location where it was activated. Because unactivated azidocoumarin continually diffuses into the focal spot, there is a buildup of activated coumarin bound to the gel at the focus. From Fig. 2 it is clear that the absorption bands of the azidocoumarin and its corresponding coumarin dye overlap, so the same excitation that activated the azide and caused the buildup of bound dye also gives rise to two-photon fluorescence. The combination of these effects manifests as an onset of fluorescence, as is shown in Fig. 3. The fluorescence initially increases linearly with time, but eventually saturates at a constant level as a steady state is achieved where the rates of binding and photobleaching of the coumarin derivatives come into balance.

Since the cross section for two-photon activation of AzC is much smaller than for two-photon fluorescence from the resulting dye, it is possible to image the written fluorescence pattern with the same technique as was used to write it, only using a lower laser power and/or faster scanning. In this mode of operation, the light is sufficient to produce detectable two-photon fluorescence, but not intense enough to cause significant photoactivation of the azidocoumarin. This is illustrated in Fig. 4, where the "VT" logo was written by with a laser power of 32 mW and a pixel dwell time of 250 μs, but the imaging was done with a laser power of 13 mW and a 13 μs pixel dwell time.

Theoretical Model of Fluorescence

The fluorescence onset in Fig. 3 results from the interplay of several effects: Photoactivation of azidocoumarin; diffusion

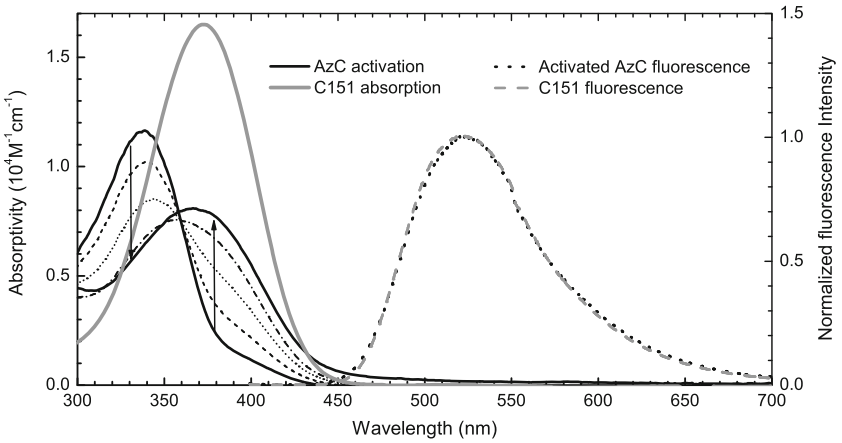

Fig. 2 Absorptivity spectra of AzC 151 in an methanolic solution and in the presence of gelatin (*black lines*) as they evolve under UV irradiation. The solid lines represent the initial (0 mJ/cm^2 UV dose) and final (5,000 mJ/cm^2 UV dose) spectra. Further UV exposure does not change the spectrum appreciably. The intermediate does are 200 mJ/cm^2, 400 mJ/cm^2 and 800 mJ/cm^2. The absorptivity spectrum of coumarin 151 is also shown (*solid grey line*). The nearly identical normalized fluorescence spectra of activated AzC151 and C151 are indicated by the *dotted black* and *dashed grey lines*, respectively

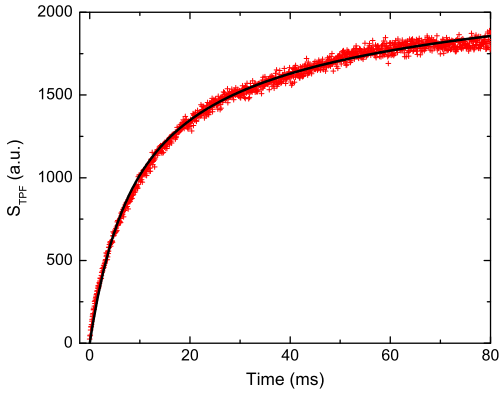

Fig. 3 Onset of two-photon fluorescence as 720 nm pulsed laser light is focused into the gel, fit to the model described in the text (color online)

of the photoactivated product through the gel; its binding to the gelatin matrix, resulting in a fluorescent dye; photobleaching of that dye; and diffusion of azidocoumarin from outside the beam to replace the photo converted azide. Since the intensity of the beam is not uniform, the photoactivation takes place at different rates at different points in the beam, and for the same reason, the contribution of each point to the signal is also different.

This is a rather complex situation to model, but it can be simplified considerably by neglecting the effects of diffusion, which is well motivated in this case. First, at the relatively low laser intensities used here, the rates of photoactivation and bleaching are sufficiently low that diffusion is a fast process by comparison. In particular, the time t_D required for a molecule to diffuse across the width of the laser beam is approximately given by $t_D \sim (2W_0)^2/D$, where $2W_0$ is the beam width, and D is the diffusion constant. The beam width is on the order of 0.5 μm, and the diffusion constant is not likely to be much smaller than 10^{-6} cm^2/s for small molecule diffusion in the gel [27]. t_D is therefore no larger than about a millisecond. Given that the fluorescence onset occurs on timescales from tens of milliseconds to several seconds, we can treat the diffusion as nearly instantaneous compared to the timescales of photoactivation and bleaching. The most important consequence of this is that we can treat the background concentration of unreacted azidocoumarin c as essentially constant and equal to its background value throughout the laser beam spot, as photoactivated AzC is rapidly replaced during the illumination.

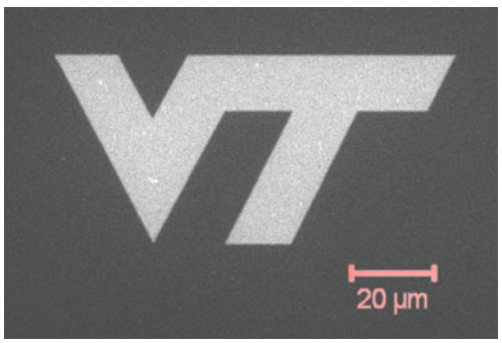

Fig. 4 Micro-patterned fluorescence created by slow scanning of the target area at high optical power, followed by readout by rapid scanning at a lower power. The latter illumination does not appreciably activate the azidocoumarin, so pattern creation and visualization can be obtained with the same laser wavelength

Moreover, the high reactivity of the photoactivated coumarin combined with the high density of binding sites provided by the gel means that we can ignore any diffusion after photoactivation, and assume that the photoactivation and binding of each AzC molecule occur at the same locations. The rate of accumulation of fluorescent dye bound to the gel is therefore proportional to the square of the local laser intensity, and the same holds true for the rate of two-photon induced photobleaching. Under those assumptions, the concentration c_f of fluorescent coumarin dye in the gel is given by the master equation

$$\frac{dc_f}{dt} = \left(\phi\beta_a c - \beta_b c_f\right) g I_\omega^2(\mathbf{r}) \tag{1}$$

where c is the background concentration of unreacted azidocoumarin, β_a and β_b are the two-photon cross sections for photoactivation and photobleaching, ϕ is the fraction of activated dye that is both fluorescent and ends up binding to the gel, and $I_\omega(\mathbf{r}) = \langle I_\omega(\mathbf{r})\rangle$ is the average light intensity distribution inside the focal spot in units of photons×cm^{-2}×s^{-1}. $g = \langle I_\omega^2\rangle \big/ \langle I_\omega\rangle^2$, or the ratio of the time-average of the square of the light intensity to the average light intensity squared. Two-photon processes scale with the former quantity, while the latter is easy to measure directly, so it is convenient to include this scale factor in the calculations. In our case, a $sech^2$ pulse shape with 150 fs FWHM and a repetition rate of 80 MHz gives g close to 5×10^4.

Assuming a spatially invariant c, Eq. (1) can be solved easily, and the two-photon fluorescence intensity (S_{TPF}) then takes the form

$$\begin{aligned} S_{TPF} &= K\beta_f \int I_\omega^2(\mathbf{r}) c_f \, d\mathbf{r} \\ &= K\phi c g \beta_f \frac{\beta_a}{\beta_b} \int I_\omega^2(\mathbf{r}) \left[1 - \exp\left(-\beta_b g I_\omega^2(\mathbf{r}) t\right)\right] d\mathbf{r}, \end{aligned} \tag{2}$$

where β_f is the cross section for two-photon fluorescence and the constant K accounts for the detection efficiency of the system. We will approximate the point spread function of the optical system with an ideal Gaussian beam:

$$\begin{aligned} I_\omega(\mathbf{r}) &= \frac{2P}{\pi h\nu W^2(z)} \exp\left(-\frac{2\left(x^2+y^2\right)}{W^2(z)}\right), \\ W^2(z) &= W_0^2\left(1 + (z/z_0)^2\right), \end{aligned} \tag{3}$$

where P is the total power of the beam, and the beam waist radius W_0 is related to the depth of focus $2z_0$ and the wavelength in the gel λ by

$$2z_0 = \frac{2\pi {W_0}^2}{\lambda}. \tag{4}$$

This is a reasonable approximation near the center of the beam spot, which is the area that dominates the two-photon fluorescence signal. This is particularly true since we are operating with the confocal aperture wide open, so that the relevant aperture in the system is the back aperture of the microscope objective, which is more than twice the beam diameter.

Physically, Eq. (2) describes an exponential approach to saturation of two-photon fluorescence due to competition between fluorescence activation and bleaching. The rate of this process is proportional to ${I_\omega}^2(\mathbf{r})$, and as a result, the saturation occurs first at the center of the beam, where the intensity is at its maximum. Locations further out see a lower light intensity, and will therefore reach saturation at later times. The net result of this is that the width of the fluorescent spot made by focusing the pulsed laser into the gel increases over time.

This can be seen in the data plotted in Fig. 5, which was obtained by illuminating a single location in the gel for a set amount of time, and then scanning across the x-y plane while measuring the two-photon fluorescence. The resulting profile is therefore $c_f * {I_\omega}^2$, or the convolution of the concentration of fluorescent dye bound to the gel with the square of the point spread function. In Fig. 5, the gel was illuminated with a 40x oil immersion objective at an optical power of 13 mW. As the illumination time is increased, the effective width of the fluorescent spot gradually increases, accompanied by a marked saturation of the fluorescence intensity, particularly at the center of the spot.

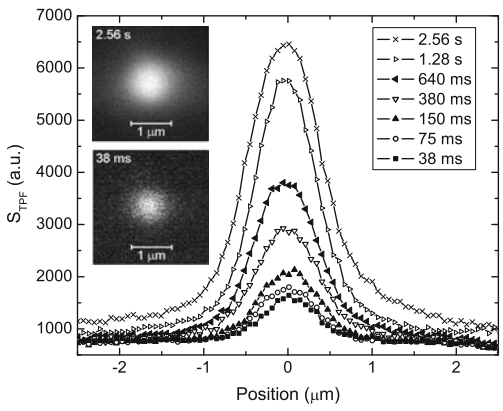

Fig. 5 Profiles of two-photon fluorescence spots that result from focusing the laser into the gel for varying amounts of time. Because fluorescence saturation occurs first at the center of the beam spot, the width of the spot increases with increasing exposure to the laser light

Scaling with Optical Power

Taking $I_\omega(\mathbf{r})$ to be Gaussian, the integral in Eq. (2) cannot be solved explicitly, but we can write it as a power series:

$$S_{\mathrm{TPF}} = K'\beta_f \frac{\beta_a}{\beta_b} \frac{gP^2}{(h\nu)^2} \sum_{n=1}^{\infty} \frac{(-1)^{n+1}}{(n+1)\pi^{2n-1}} \frac{(4n-1)!!}{n!(2n)!} \left(\frac{gP^2\beta_b}{(h\nu)^2 {W_0}^4} t \right)^n, \tag{5}$$

where, for brevity's sake, we define $K' = K\phi c/\lambda$. The integral takes on a simpler form at short and long times. At short times, photobleaching is not a factor, the fluorescence increases linearly in time, and Eq. (2) can be approximated as

$$S^0_{\mathrm{TPF}} \approx K' g^2 \lambda \beta_f \beta_a t \int {I_\omega}^4(\mathbf{r}) \mathrm{d}\mathbf{r} = \frac{3K' g^2 \beta_f \beta_a}{4\pi (h\nu W_0)^4} P^4 t. \tag{6}$$

At long times, the fluorescence saturates, tending to a constant value

$$S^\infty_{\mathrm{TPF}} = K' \lambda g \beta_f \frac{\beta_a}{\beta_b} \int {I_\omega}^2(\mathbf{r}) \mathrm{d}\mathbf{r} = K' g \beta_f \frac{\beta_a}{\beta_b} \frac{\pi}{(h\nu)^2} P^2. \tag{7}$$

In other words, the initial slope of the activation curve will be proportional to P^4, while the fluorescence signal at saturation is proportional to P^2. The onset of fluorescence is due to a combination of two-photon activation and two-photon fluorescence, which explains the P^4 scaling of the initial slope. Saturation of the fluorescence is reached at a value that depends on the ratio of the activation and photobleaching cross sections, and since both of those processes have the same P^2 dependence on optical power, the quantity of optically active fluorophores at saturation is independent of optical power, at least to first approximation. For that reason, S^∞_{TPF} is governed only by a two-photon fluorescence process, and should scale as P^2.

As can be seen in Fig. 6a, the initial slope of the observed two-photon fluorescence obeys these scaling laws quite well, with an exponent of 4.18. The deviation from the exact value of 4 can be attributed to the nonlinearity of our optical power meter and the difficulty of accurately measuring the initial slope of a curve over six orders of magnitude of dynamic range. As for S^∞_{TPF}, it does obey a power law, but the observed exponent (Fig. 6b) is only 1.34, well below the predicted value of 2.

To help determine the source of this deviation from the model, we optically activated AzC in a volume of the gel, creating a concentration c_f^0 of fluorescent dye within the volume. Two-photon fluorescence ($S_{2\omega}$) was then measured by rapidly scanning through this region while varying the

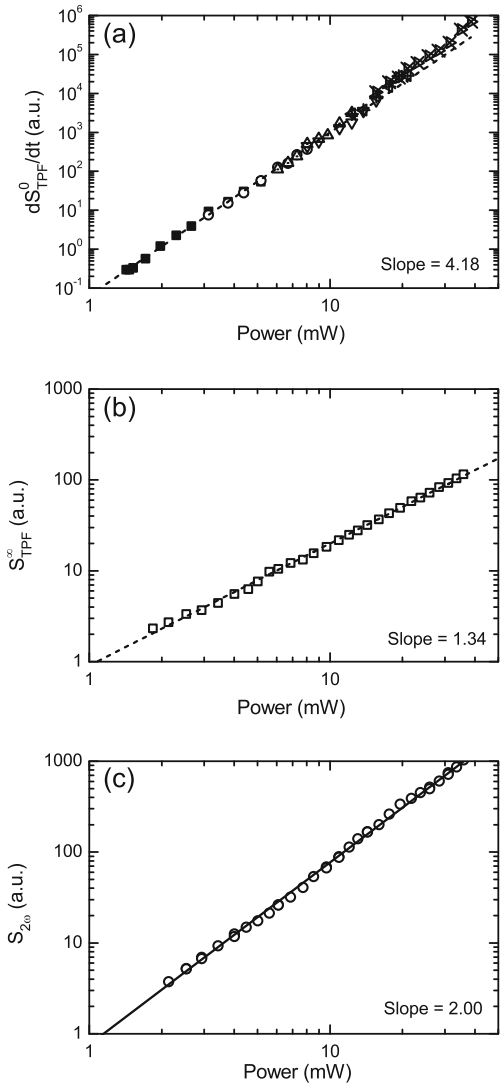

Fig. 6 **a** Log plot of the initial slope of the two-photon fluorescence onset as a function of incident optical power. The exponent is approximately four because the onset results from the combination of two-photon activation and two-photon fluorescence, each of which contributes a factor of P^2 to the power dependence. The different marker styles correspond to different settings for the detector gain and integration time. **b** Log plot of the steady state two-photon fluorescence signal at long times vs. incident optical power. **c** Log plot of the two-photon fluorescence signal from a previously photoactivated volume of the gel. In contrast to plots (a) and (b), the beam is scanned rapidly to negate the effect of photobleaching

laser power. Neither photoactivation nor photobleaching affect $S_{2\omega}$, which is given by

$$S_{2\omega} = \frac{K\phi c_f^0}{\lambda} g\beta_f \frac{\pi}{(h\nu)^2} P^2. \quad (8)$$

As shown in Fig. 6c, the P^2 scaling is actually observed in this case, which means that the observed fluorescence is indeed due to two-photon fluorescence, and the deviation from Eq. (7) is due to some other factor.

Effect of Damage to the Gel

Clearly, some process other than two-photon photobleaching is at work suppressing the fluorescence from the activated azidocoumarin, at least at longer time scales. This can also be seen from the fluorescence spot scans shown in Fig. 7a. Here, the gel was illuminated at 3.4 mW for 164 s, and 38 mW for 1.27 s. $t_{ill}P^2$, the illumination time multiplied by the square of the optical power, is approximately the same in both cases. If Eq. (2) were accurate at all time scales, we would expect the same amount of photoactivation and photobleaching to have taken place in both cases, and the two resulting traces in Fig. 7a would be very similar. Instead, only the fluorescence pattern at low illumination power shows the expected peak. At high power, a ring of fluorescence is seen instead, and the peak fluorescence is much lower than in the low power case. If the fluorescence quenching were due exclusively to a two-photon process we would expect to see a flattening of the peak at long illumination times as the fluorescence everywhere approaches the same value. The ring-like shape must then be attributed to a process that scales faster with optical power than P^2. This could include multi-photon processes as well as optically or thermo-optically induced changes in the gelatin matrix.

Once a ring-like structure such as is shown in the insert in Fig. 7a has been created, it is permanent. Illuminating the same location at low optical power for a long time still results in a ring-like fluorescence pattern rather than the single peak. We therefore conclude that the additional reduction in two-photon fluorescence seen at high powers and long times is due to damage or phase change in the gel induced by the high optical power density. Gelatin solutions have a sol–gel transition temperature near 28 °C [26], and the gelatin-water-alcohol mixture we are using is metastable at room temperature. It is then quite reasonable that intense light can trigger local phase separation or other changes in the gel if applied for a sufficient amount of time. In spite of this, the initial slope of the two-photon fluorescence onset has the predicted dependence on optical power over a wide range of powers, which indicates that at short exposure times, damage to the gel is not yet significant, and the model presented above is accurate.

To model the degradation, we will make three simplifying assumptions: (1) The rate of degradation depends only on the local light intensity $I_\omega(\mathbf{r})$. (2) There is a threshold for degradation, so that if the light intensity does not exceed some value I_m, no degradation takes place. (3) Wherever $I_\omega(\mathbf{r})>I_m$, the fluorescence will

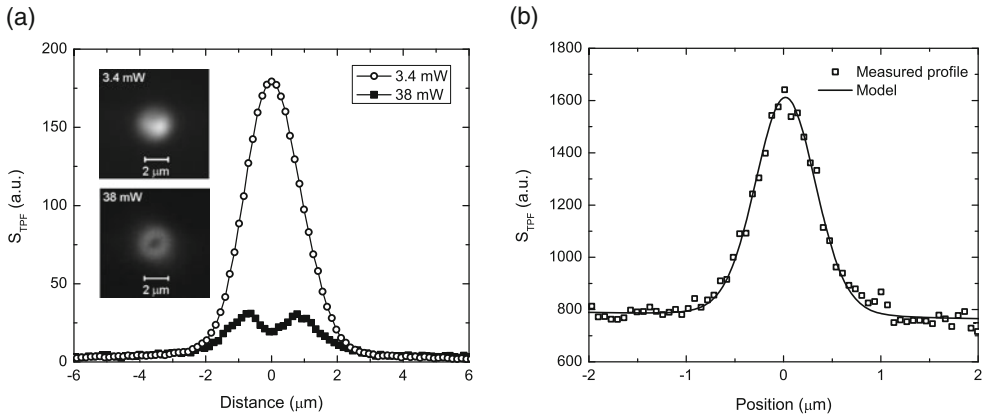

Fig. 7 **a** Two-photon fluorescence profiles resulting from illuminating the gel at low power for a long time (3.4 mW, 164 s) and at high power for a shorter time (38 mW, 1.27 s). Both illuminations should result in the same amount of azidocoumarin activation, but much less fluorescence is seen in the high power case due to damage inflicted on the gel by the light. **b** Two-photon fluorescence profile obtained at low power and short illumination time in order to minimize saturation. The *solid line* is a fit to the autocorrelation function of a Gaussian beam profile, yielding a beam radius of 0.56 μm

eventually go to 0. Denoting $P_m = \frac{1}{2}\pi(h\nu)^2 W_0^2 \cdot I_m$, we have, when $P > P_m$,

$$S_{\mathrm{TPF}}^{\infty} = K'\lambda g\beta_f \frac{\beta_a}{\beta_b} \int\limits_{I_\omega < I_m} {I_\omega}^2(\mathbf{r})\mathrm{d}\mathbf{r} =$$

$$= K' g\beta_f \frac{\beta_a}{\beta_b} \frac{2}{(h\nu)^2}\left[\frac{1}{3}(P+2P_m)\sqrt{P_m(P-P_m)} + P^2 \arctan\sqrt{\frac{P_m}{P-P_m}}\right]$$

$$\xrightarrow{P \gg P_m} K' g\beta_f \frac{\beta_a}{\beta_b} \frac{8}{3(h\nu)^2} P_m^{1/2}\ P^{3/2}, \tag{9}$$

while for $P \leq P_m$, Eq. (7) is still valid. The 3/2 exponent in the optical power dependence in Eq. (9) is not exactly what is observed, but it is close enough to our observations that the difference could be due to measurement errors, particularly since Eq. (9) can be fit quite well with a function proportional to $P^{1.43}$ when $1 < P/P_m \lesssim 20$. It is also likely that the assumptions we made to arrive at Eq. (9) are not entirely valid for our situation, although they are a good starting point as they lead to an easily solvable model that is largely consistent with our observations.

Estimating the Two-Photon Photobleaching Cross Section

We can further verify the validity of our model by fitting the function given by Eq. (5) to the fluorescence onset curve. As can be seen from Fig. 3, the fit is quite good, at least for short times. For longer times, the model deviates significantly from the data, as expected (not shown). Not only does gel damage start to set in over time, but since the fluorescence from the center of the beam spot saturates first, the evolution of the fluorescence at later times depends on the details of the point spread function farther away from the focus, where the Gaussian approximation no longer is particularly good.

With sufficient knowledge of the point spread function, we can use the fit in Fig. 3 to measure the two-photon bleaching rate of the activated azidocoumarin. This is not the main purpose of this paper, and a high accuracy measurement would be better performed in a thin film of gel, and using a low N.A. laser beam, for which the approximations impart less error, and the paraxial approximation can be used. For illustrative purposes, we will still carry out the calculation with the data available here, but we emphasize that there is a fairly high level of uncertainty to the resulting estimates.

The fit is done by scaling the model along both the time and intensity axes to obtain the best agreement with the data. The scale factor in time (γ) is, from Eq. (5)

$$\gamma = \frac{gP^2\beta_b}{(h\nu)^2 {W_0}^4}, \tag{10}$$

where all parameters except β_b can be measured directly. The source of the greatest uncertainty is the fourth-power dependence on the beam spot radius. More generally, the true point spread function of the optical system must be well known if we are to be able to accurately determine β_b. For that reason, we will only provide a rough estimate here, based on our Gaussian approximation of the beam profile.

We can estimate W_0 using the fluorescence spot scans such as those in Fig. 5. At sufficiently low power and short

illumination time, before fluorescence saturation sets in, the spot profile will be proportional to the autocorrelation function of the square of the laser intensity

$$\left(I_\omega{}^2 * I_\omega{}^2\right)[x, y = z = 0] \propto \int_{-\infty}^{\infty} \frac{\exp\left(-\frac{2x^2}{W_0{}^2(1+z^2)}\right)}{(1+z^2)^3}\, dz, \qquad (11)$$

which can be solved numerically and fit to the data to extract W_0, as has been done in Fig. 7b. The fit gives us that W_0= 0.56 μm. With an incident power of 8.3 mW, we find a scale factor of about γ=294 s^{-1}. Taking g to be 5×10^4, Eq. (10) yields an estimate of β_b~0.006 G.M. (10^{-50} cm^4s).

Quantum Yield of Photobleaching

In Fig. 8, we have plotted the two-photon fluorescence cross section of C151 vs. wavelength (open diamonds). This was obtained by measuring the two-photon fluorescence at different excitation wavelengths while maintaining a constant laser power. The data was then scaled to match literature values for the two-photon absorption cross section (δ) in C151 [28], and taking the quantum yield of fluorescence (Φ_f) to be 0.582 [28], from which we can extract $\beta_f = \Phi_f\delta$.

One- and two-photon absorption processes have quite different selection rules and in general couple different electronic states, but in a highly asymmetric molecule, most electronic states are strongly hybridized, and both processes are likely to couple the same states, albeit with varying oscillator strengths. We therefore also plot the linear absorption spectrum for C151 in Fig. 8. By plotting the laser wavelengths against two times the value of the absorption wavelengths, we get good agreement between linear and nonlinear spectra, indicating that both one- and two-photon absorption do indeed occur into the same electronic state and that in the examined wavelength range, those states are fluorescent. Given this, we estimate that $\beta_f \approx$ 26 G.M. for C151 at 720 nm.

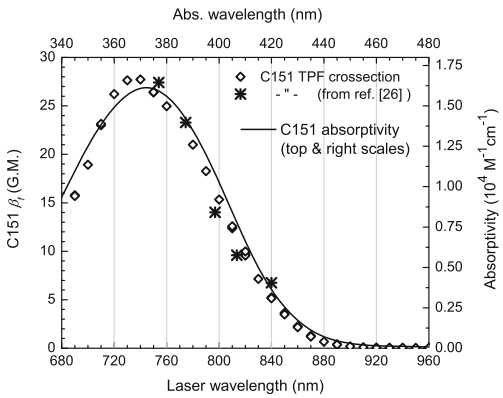

Fig. 8 (left and bottom axes): *Open diamonds* plot the two-photon fluorescence cross section (β_f) of C151 dissolved at 1 mM concentration in a gelatin gel. The data was obtained by measuring the two-photon fluorescence intensity as a function of laser wavelength, and scaling to agree with data from ref. [28], indicated by *stars*. (top and right axes): The *solid line* is the absorptivity spectrum of coumarin 151. The two horizontal scales differ by a factor of two, and the good agreement between the datasets indicate that one- and two-photon absorption occur into the same electronic state

We do not know the abundance of the reaction products in the gel after photoactivation of AzC151, although the spectra plotted in Fig. 2 provides some indication. Since the absorption of the photoactivated dye peaks at the same wavelength than for C151, it is likely that **5** has a β_f value quite similar to C151 at 720 nm. From this we can estimate the quantum yield of photobleaching $\Phi_b = \Phi_f \frac{\beta_b}{\beta_f} \approx 1.3 \times 10^{-4}$, which is consistent with values obtained for other coumarin dyes under single photon excitation [29].

Conclusion

We have studied the onset of two-photon fluorescence in azidocoumarin 151 contained in a gelatin matrix and illuminated by focused femtosecond laser light. Since the photoactivated intermediary is highly reactive, it binds to the gelatin matrix close to the location of its creation. This makes it possible to create arbitrary three-dimensional patterns of fluorescence, similarly to the way two-photon exposure of a photoresist can be used to create arbitrary three-dimensional geometries.

A model based on a Gaussian approximation of the beam profile describes the onset of fluorescence quite well at short time scales, but fails at longer times, likely due to a combination of damage to the gel and the inadequacy of the Gaussian approximation when outlying areas of the beam spot dominate the behavior of the two-photon fluorescence. When the gel damage is incorporated into the model, most of the discrepancy with experiment is removed. The success of the model, especially at short times, makes it possible to extract an estimate for the two-photon cross section for photobleaching of the coumarin dye. As the beam waist is known to insufficient accuracy, there is a high degree of uncertainty in this estimate, but this could be remedied with better knowledge of the microscope point spread function and a more favorable sample geometry.

The model used here does not take diffusion into account, which is appropriate given the experimental conditions. In situations when diffusion does have a significant effect on the physics, the functional dependence of fluorescence onset could potentially be used to measure the diffusion constant, offering an alternative to the Fluorescence Recovery After Photobleaching (FRAP) technique. [30]

Acknowledgements This work was funded by a grant from the National Science Foundation (agreement CBET-0756693), the Institute for Critical Technology and Applied Science (ICTAS) and by a grant from the Thomas F. Jeffress and Kate M. Jeffress Memorial Trust.

References

1. Betzig E, Patterson GH, Sougrat R, Lindwasser OW, Olenych S, Bonifacino JS, Davidson MW, Lippincott-Schwartz J, Hess HF (2006) Imaging intracellular fluorescent proteins at nanometer resolution. Science 313(5793):1642–1645. doi:10.1126/science.1127344
2. Hess ST, Girirajan TPK, Mason MD (2006) Ultra-high resolution imaging by fluorescence photoactivation localization microscopy. Biophys J 91(11):4258–4272. doi:10.1529/biophysj.106.091116
3. Zhuang XW, Rust MJ, Bates M (2006) Sub-diffraction-limit imaging by stochastic optical reconstruction microscopy (STORM). Nat Methods 3(10):793–795. doi:10.1038/nmeth929
4. Lukyanov KA, Chudakov DM, Lukyanov S, Verkhusha VV (2005) Photoactivatable fluorescent proteins. Nat Rev Mol Cell Biol 6(11):885–891 doi:10.1038/nrm1741
5. Patterson GH (2011) Highlights of the optical highlighter fluorescent proteins. J Microsc 243(1):1–7. doi:10.1111/j.1365-2818.2011.03505.x
6. Tinnefeld P, Vogelsang J, Steinhauer C, Forthmann C, Stein IH, Person-Skegro B, Cordes T (2010) Make them blink: probes for super-resolution microscopy. Chemphyschem 11(12):2475–2490. doi:10.1002/cphc.201000189
7. Warther D, Gug S, Specht A, Bolze F, Nicoud JF, Mourot A, Goeldner M (2010) Two-photon uncaging: new prospects in neuroscience and cellular biology. Bioorg Med Chem 18(22):7753–7758. doi:10.1016/j.bmc.2010.04.084
8. Han G, Mokari T, Ajo-Franklin C, Cohen BE (2008) Caged quantum dots. J Am Chem Soc 130(47):15811–15813. doi:10.1021/ja804948s
9. Lord SJ, Lee HLD, Samuel R, Weber R, Liu N, Conley NR, Thompson MA, Twieg RJ, Moerner WE (2010) Azido push-pull fluorogens photoactivate to produce bright fluorescent labels. J Phys Chem B 114(45):14157–14167. doi:10.1021/jp907080r
10. Thevenin BJM, Shahrokh Z, Williard RL, Fujimoto EK, Kang JJ, Ikemoto N, Shohet SB (1992) A novel photoactivatable crosslinker for the functionally-directed region-specific fluorescent labeling of proteins. Eur J Biochem 206(2):471–477 doi:10.1111/j.1432-1033.1992.tb16949.x
11. Vaziri A, Tang JY, Shroff H, Shank CV (2008) Multilayer three-dimensional super resolution imaging of thick biological samples. Proc Natl Acad Sci USA 105(51):20221–20226. doi:10.1073/pnas.0810636105
12. Zhuang XW, Huang B, Wang WQ, Bates M (2008) Three-dimensional super-resolution imaging by stochastic optical reconstruction microscopy. Science 319(5864):810–813. doi:10.1126/science.1153529
13. Juette MF, Gould TJ, Lessard MD, Mlodzianoski MJ, Nagpure BS, Bennett BT, Hess ST, Bewersdorf J (2008) Three-dimensional sub-100 nm resolution fluorescence microscopy of thick samples. Nat Methods 5(6):527–529 doi:10.1038/nmeth.1211
14. Schmidt R, Wurm CA, Jakobs S, Engelhardt J, Egner A, Hell SW (2008) Spherical nanosized focal spot unravels the interior of cells. Nat Methods 5(6):539–544 doi:10.1038/nmeth.1214
15. LaFratta CN, Fourkas JT, Baldacchini T, Farrer RA (2007) Multiphoton fabrication. Angew Chem Int Ed 46(33):6238–6258 doi:10.1002/anie.200603995
16. Zhou WH, Kuebler SM, Braun KL, Yu TY, Cammack JK, Ober CK, Perry JW, Marder SR (2002) An efficient two-photon-generated photoacid applied to positive-tone 3D microfabrication. Science 296(5570):1106–1109 doi:10.1126/science.296.5570.1106
17. Allonas X, Fouassier JP, Kaji M, Miyasaka M, Hidaka T (2001) Two and three component photoinitiating systems based on coumarin derivatives. Polymer 42(18):7627–7634 doi:10.1016/S0032-3861(01)00275-0
18. Monroe BM, Weed GC (1993) Photoinitiators for free-radical-initiated photoimaging systems. Chem Rev 93(1):435–448 doi:10.1021/cr00017a019
19. Wu SK, Zhang JK, Fouassier JP, Burr D (1989) A transient study on the ketocoumarin derivatives II. The triplet quenching of ketocoumarin by different monomers and amines. Photogr Sci Photochem 2:47–54
20. Wang T, Zhao YX, Shi MQ, Wu FP (2007) The synthesis of novel coumarin dyes and the study of their photoreaction properties. Dye Pigment 75(1):104–110. doi:10.1016/j.dyepig.2006.04.019
21. Di Lullo GA, Sweeney SM, Korkko J, Ala-Kokko L, San Antonio JD (2002) Mapping the ligand-binding sites and disease-associated mutations on the most abundant protein in the human, type I collagen. J Biol Chem 277(6):4223–4231. doi:10.1074/jbc.M110709200
22. Lee SJ, Liu J, Oh SH, Soker S, Atala A, Yoo JJ (2008) Development of a composite vascular scaffolding system that withstands physiological vascular conditions. Biomaterials 29 (19):2891–2898. doi:10.1016/j.biomaterials.2008.03.032
23. Schnapp KA, Poe R, Leyva E, Soundararajan N, Platz MS (1993) Exploratory photochemistry of fluorinated aryl azides - implications for the design of photoaffinity-labeling reagents. Bioconjug Chem 4(2):172–177 doi:10.1021/bc00020a01
24. Feng KS, Mahdavianary F, Partch RE, Li YZ (1995) Photochemical reactions of azidocoumarins. Photochem Photobiol 62(5):813–817 doi:10.1111/j.1751-1097.1995.tb09141.x
25. Barral K, Moorhouse AD, Moses JE (2007) Efficient conversion of aromatic amines into azides: a one-pot synthesis of triazole linkages. Org Lett 9(9):1809–1811 doi:10.1021/ol070527h
26. Tanaka T, Swislow G, Ohmine I (1979) Phase-separation and gelation in gelatin gels. Phys Rev Lett 42(23):1556–1559 doi:10.1103/PhysRevLett.42.1556
27. Friedman L (1930) Diffusion of non-electrolytes in gelatin gels. J Am Chem Soc 52(4):1305–1310. doi:10.1021/ja01367a002
28. Fischer A, Cremer C, Stelzer EHK (1995) Fluorescence of coumarins and xanthenes after 2-photon absorption with a pulsed titanium-sapphire laser. Appl Opt 34(12):1989–2003 doi:10.1364/AO.34.001989
29. Eggeling C, Widengren J, Rigler R, Seidel CAM (1998) Photobleaching of fluorescent dyes under conditions used for single-molecule detection: evidence of two-step photolysis. Anal Chem 70(13):2651–2659 doi:10.1021/ac980027p
30. Sprague BL, Pego RL, Stavreva DA, McNally JG (2004) Analysis of binding reactions by fluorescence recovery after photobleaching. Biophys J 86(6):3473–3495. doi:10.1529/biophysj.103.026765